INHIBITOR EVOLUTION: HOW DRUG DESIGN EVOLVED TO OVERCOME MUTATION MECHANISMS

Anonymous authors
Paper under double-blind review

ABSTRACT

Targeting the epidermal growth factor receptor (EGFR) in cells with tyrosine kinase inhibitors (TKIs) is an established strategy to block oncogenic phosphorylation cascades and tumor growth in non-small cell lung cancer (NSCLC). However, tumors frequently develop resistance through the T790M gatekeeper mutation, mitigating the effect of early-generation TKIs. Consequently, later generations of TKIs have been developed to combat these mutations. Our experiment computationally compared five TKIs spanning three drug generations (Erlotinib, Gefitinib, Afatinib, Dacomitinib, and Osimertinib) against wild-type and T790M mutant EGFR to provide an effective evaluation of TKI-generation evolution. Standardized molecular docking via AutoDock Vina was utilized for each TKI-receptor combination, revealing minimal free energy changes across TKI generation and receptor state ($\Delta\Delta G = -0.30$ to $+0.46$ kcal/mol), demonstrating that docking scores fail to explain inhibitor generation efficacy differences. Consequently, Python Molecule 3D Rendering (PyMOL) and Protein-Ligand Interaction Profiling (PLIP) analysis determined Third-generation TKIs optimally increased gatekeeper clearance distance when met with the mutated receptor (3.07 Å to 4.31 Å) to remain in an ideal position to block unwanted cell signals while increasing hydrophobic contact (2 to 4 contacts) to block ATP and oncogenic phosphorylation cascades, which the first-generation TKIs failed to achieve. Ultimately, this study demonstrates the specific structural shifts that Third-generation TKIs utilize to remain more effective than first-generation TKIs when faced with mutated receptors.

1 INTRODUCTION

Lung cancer remains as one of the leading causes of death, with non-small cell lung cancer (NSCLC) remaining as one of the most prevalent and dangerous types. NSCLC functions through mutations in the epidermal growth factor receptor (EGFR) causing oncogenic cell growth and proliferation (Lynch et al., 2004; Pao et al., 2005). Over time, tyrosine kinase inhibitors (TKIs) have been developed to combat mutated EGFRs. Researchers have developed various generations of TKIs, each with specific properties designed to nullify the effects of the EGFR mutations. Early TKI generations resulted in severe limitations whereas later TKI generations were able to efficiently combat EGFR mutations. However, the exact mechanisms and biological framework as to how these later TKI generations functioned to combat EGFR mutations tend to be unclear, often simply being seen as a form of abstraction. To clarify how TKI design evolved with each generation to combat mutated receptors, this study employs three underlying analysis methods to provide an effective evaluation of TKI-generation evolution: standardized molecular docking, to calculate binding energy (ΔG) shifts across inhibitor generation and receptor states; PyMOL 3D rendering, to visualize TKI active site accommodations and alignment at a molecular level; and PLIP analysis, to map specific non-covalent contact changes between target inhibitors and receptors. By integrating these methods, our study aims to clarify the precise biological mechanisms driving TKI-generation adaptation at the molecular level.

2 LITERATURE REVIEW

In non-small cell lung cancer (NSCLC), researchers have utilized Tyrosine Kinase Inhibitors (TKIs) in an attempt to inhibit the epidermal growth factor receptor (EGFR) and block abnormal cell signals

Reviewers: please read the Reviewer Guidelines (iclr.cc/Conferences/2027/ReviewerGuidelines) and the AI Policy for Reviewers (iclr.cc/Conferences/2027/AIPolicyForReviewers). If you used AI to expand, edit, or polish your review, please provide the input text to the LLM. Better still, consider skipping the LLM and submitting your original text: we, and the authors, are much more interested in your unedited thoughts than in what an LLM has to say. AI-assisted or not, you are putting your name and reputation behind your review: LLM-generated falsehoods, hallucinations or misrepresentations are subject to disciplinary action, which may include desk-rejecting all papers you have authored.

and pathways (Lynch et al., 2004; Ward et al., 2013). The first generation of TKIs developed (Erlotinib and Gefitinib) competitively inhibited the ATP-binding site of mutant EGFR receptors, though this development was shortly nullified due to the emergence of the T790M gatekeeper mutation that substituted threonine with methionine to increase ATP receptor affinity along with introducing steric hindrance to effectually combat this generation of TKIs (Kobayashi et al., 2005; Lynch et al., 2004; Pao et al., 2005; Yun et al., 2008).

In response to this T790M resistance, second-generation TKIs (Afatinib and Dacomitinib) were created specifically to form covalent linkages at residue Cys797, which would effectively lock the inhibitor in place and not allow ATP or other molecules to occupy the active site (Li et al., 2008; Solca et al., 2012). Unfortunately, due to dose-limiting toxicities, this generation of TKIs failed to achieve a meaningful therapeutic window: drug levels were either so high that the toxicity became unbearable for normal tissues or too low so that the drug posed no effect against the mutation (Cross et al., 2014; Engelman et al., 2007; Li et al., 2008). As a result, they failed to effectively combat T790M (Li et al., 2008; Zhou et al., 2009).

This would lead to the development of third-generation TKIs (Osimertinib) and its mutant-selective breakthrough of targeted Cys797 covalent binding. This generation would target the T790M variant while sparing wild-type EGFR, resulting in high therapeutic efficacy along with minimal toxicity in healthy unmutated tissues (Cross et al., 2014; Finlay et al., 2014; Mok et al., 2017; Ward et al., 2013).

Despite the clear hierarchy in TKI generation, the precise structural mechanisms of TKI generation evolution remains unclear (Lynch et al., 2004). Previous studies rely on simplified metrics such as scalar binding energy-docking scores (ΔG), which fail to specifically target the active-site accommodation of the TKI generations. Our study therefore aims to address this ambiguity by providing empirical structural evidence specifically detailing TKI generation growth against the T790M gatekeeper mutant receptor.

3 METHODOLOGY

This section details the specific methodology and architecture used to effectively simulate and validate the impacts of the EGFR T790M gatekeeper mutation across three generations of TKIs. All experimental code is publicized for replication (Anonymous Author(s), 2026).

3.1 EXPERIMENTAL DESIGN

In order to evaluate the structural impacts of the EGFR T790M gatekeeper mutation against inhibitor generations, we first downloaded the wild-type (PDB: 1M17) and mutant EGFR receptors from the RCSB Protein Data Bank along with five representative inhibitors across three generations (First-generation: Erlotinib, Gefitinib; Second-generation: Afatinib, Dacomitinib; Third-generation: Osimertinib) obtained from PubChem in standard .SDF file format.

Preparing the receptors for docking, we removed water molecules, crystallization ions, and heteroatoms; this ensures the active site is unblocked for either inhibitors or ATP to bind, avoiding unnecessary electrostatic and steric interference. All five inhibitors underwent conformational sampling across approximately 15 distinct initial rotamer conformers using the MMFF94 force field, standardizing the initial energy state for each inhibitor to ensure no inhibitor gains an artificial higher energy state before docking.

Ensuring consistent spatial 3D evaluation of inhibitor-receptor interactions, we applied a fixed uniform grid box with dimensions $(20.0\ \text{Å} \times 20.0\ \text{Å} \times 20.0\ \text{Å})$ across the wild-type and mutant receptors to eliminate volume sampling bias. We then calculated optimal grid box centers by extracting the 3D geometric centroid of the co-crystallized ligand bound within each respective active site, determining the following coordinates:

After these setup steps, we utilized molecular docking via AutoDock Vina v1.2.5 across all receptor-inhibitor pairs using 15 independent seeds and an exhaustiveness level of 16 to calculate mean binding energy ΔG against each inhibitor's receptor type.

Following docking, top-scoring pose complexes were passed through the Protein-Ligand Interaction Profiler (PLIP) to systematically map non-covalent inhibitor-receptor interactions, specifically

Active Site Grid Box Center Coordinates

Receptor Target	X**-Center (Å)**	Y**-Center (Å)**	Z**-Center (Å)**
Wild-Type (PDB: 1M17)	23.570	9.772	59.367
Mutant (T790M)	-12.458	29.144	36.837

tracking hydrogen bond retention rates and hydrophobic interaction counts. These interactions were documented to evaluate how H-bond changes and non-polar packing corresponded to generational differences in inhibitor binding affinity.

As a final metric to determine the cause of inhibitor generation differences, PyMOL 3D active site visual analysis was conducted from PLIP complexes to evaluate spatial fitting changes introduced by the mutant receptor's methionine substitution, where distance was evaluated from the nearest receptor side-chain atom to the nearest inhibitor atom.

3.2 Computational Setup

The computational hardware specifications utilized in our experiment along with estimated execution times are listed below:

System Performance Specifications and Execution Times

Performance Tier	**CPU (Processor)**	**RAM**	**Storage**	**Est. Execution Time**
Minimum Specs *(Lowest required)*	Quad-Core CPU (4 threads)	8 GB	5 GB HDD	∼3.0–4.5 Hours (∼10–15 min/pair)
Standard Specs *(Study Benchmark)*	**Intel Core Ultra 9 (16 Cores / 16 Threads)**	**32 GB LPDDR5**	**NVMe SSD**	**∼45–60 Minutes (∼2–3 min/pair)**
Optimal Specs *(HPC / Workstation)*	32+ Core AMD EPYC / Intel Xeon	64+ GB DDR5	High-Speed NVMe	∼10–15 Minutes (<30 sec/pair)

Note: PLIP and PyMOL analysis are light processing metrics that require significantly less computational power. Meeting the hardware requirements for our docking script is sufficient to ensure replication of these metrics.

3.3 Evaluation metrics

In order to effectively address inhibitor affinity along with empirical biological relevance, the following evaluation metrics were established.

Binding Energy (ΔG) and Energy Shifts ($\Delta\Delta G$). Our docking script effectively calculates the mean free binding energy (ΔG) across 15 seeds for each inhibitor-receptor interaction. With these values, we calculated the mutant-induced energy shift ($\Delta\Delta G$) for each inhibitor through the following formula:

$$\Delta\Delta G = \Delta G_{\text{T790M}} - \Delta G_{\text{wild-type}} \tag{1}$$

Note that a positive $\Delta\Delta G$ indicates a loss in binding while a negative $\Delta\Delta G$ indicates increased binding affinity.

Pearson r & Spearman ρ. In order to cross-reference our simulation predictions against preexisting data, our predicted $\Delta\Delta G$ data was compared against IC_{50} ratios.

The Pearson Correlation Coefficient (r), which measures the linear relationship between predicted binding energy shifts ($\Delta\Delta G$) and experimental cellular resistance, was calculated from the following equation:

$$r = \frac{\sum(x_i - \bar{x})(y_i - \bar{y})}{\sqrt{\sum(x_i - \bar{x})^2 \sum(y_i - \bar{y})^2}} \tag{2}$$

The Spearman Rank Correlation Coefficient (ρ), measuring monoatomic rank agreement to evaluate if the inhibitors are ranked correctly by relative resistance, was calculated from the following equation:

$$\rho = 1 - \frac{6 \sum d_i^2}{n(n^2 - 1)} \tag{3}$$

In both equations, $\bar{x}$ = average computed energy shift ($\Delta\Delta G$), x_i = computed energy shift ($\Delta\Delta G$), $\bar{y}$ = average IC_{50} ratio, y_i = IC_{50} ratio, d_i = difference between paired ranks, and n = # evaluated inhibitors (5).

Non-Covalent Interaction Fingerprints. Top-scoring pose complexes were evaluated using Protein-Ligand Interaction Profiler (PLIP) to capture binding mechanisms that traditional energy binding (ΔG) values miss. These non-covalent interaction metrics include **Hinge Hydrogen Bonding**, which tracks the binary retention of the crucial hydrogen bond at Met793, as well as **Hydrophobic Contacts** which quantify total contact counts.

Spatial Distance. Active-site 3D rendering was conducted in PyMOL for a visual on steric hindrance. The clearance distance was measured from the nearest receptor side-chain to the nearest inhibitor atom.

4 RESULTS

Table 1: Docking ΔG and $\Delta\Delta G$ scores

Inhibitor	Target	Wildtype Mean (ΔG) ± SD	T790M Mean (ΔG) ± SD	Score Shift ($\Delta\Delta G$)
Erlotinib	1st Gen	-7.04 ± 0.12	-7.34 ± 0.04	-0.30
Gefitinib	1st Gen	-9.18 ± 0.52	-9.09 ± 0.02	+0.09
Afatinib	2nd Gen	-8.66 ± 0.15	-8.20 ± 0.02	+0.46
Dacomitinib	2nd Gen	-8.46 ± 0.05	-8.60 ± 0.11	-0.14
Osimertinib	3rd Gen	-8.15 ± 0.16	-8.24 ± 0.08	-0.08

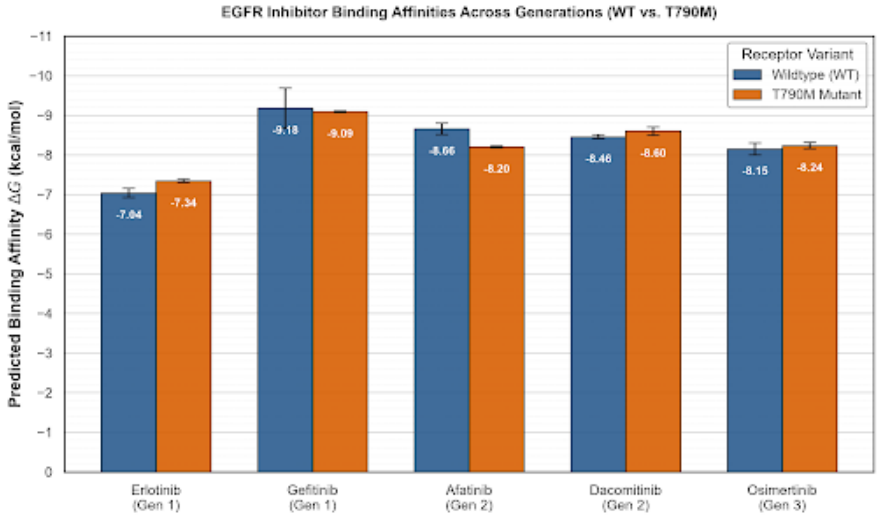


Figure 1: EGFR Inhibitor Binding Affinities Across Generations (WT vs. T790M)

Shown in Table 1 and Figure 1 is the mean binding energy (ΔG) and mean change in binding energy ($\Delta\Delta G$) scores for each inhibitor against the wild-type and mutant receptor, found through molecular docking of 15 seeds. These scalar binding energy calculations exhibit narrow thermodynamic variance across inhibitor classes. For all 5 inhibitors, $\Delta\Delta G$ hovered within a narrow margin of -0.30 to

+0.46 kcal/mol. Based strictly from this docking's binding energy scoring, first-generation inhibitors appear to maintain near-identical thermodynamic binding potential as second-generation and third-generation inhibitors. This finding demonstrates that global scalar scoring lacks the ability to show and explain how 3rd gen inhibitors retain more binding energy than 1st gen inhibitors in mutant receptors.

Figure 2: Cross-Validation across Literature IC_{50} data

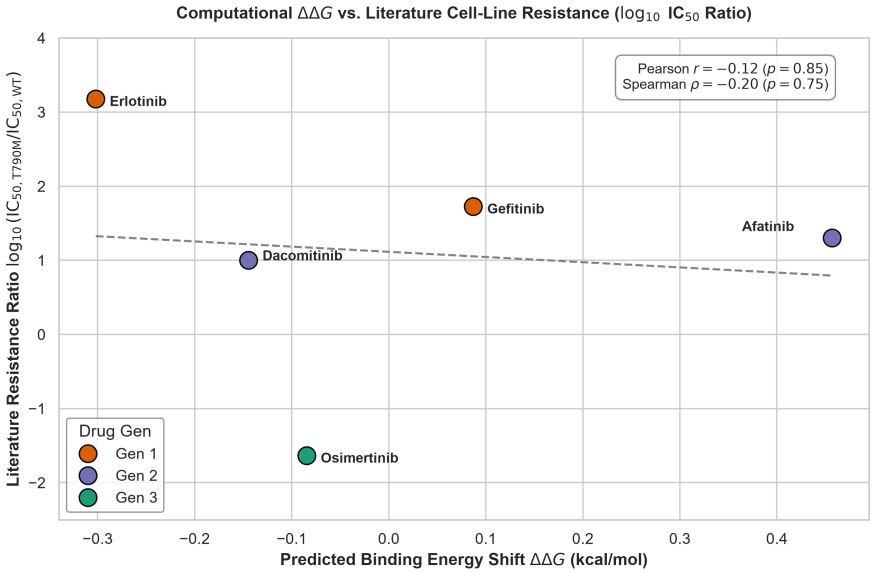


Table 2: Cross-Validation across Literature IC_{50} data

Inhibitor	Gen	Wildtype (ΔG)	T790M (ΔG)	Score Shift ($\Delta\Delta G$)	Wildtype IC_{50} (nM)	T790M IC_{50} (nM)	IC_{50} Fold-Change	$Log_{10}(IC_{50}$ Fold-Change)
Erlotinib	Gen 1	-7.04	-7.34	-0.30	2.00	3000.00	1500.00	3.18
Gefitinib	Gen 1	-9.18	-9.09	0.09	15.50	823.30	53.12	1.73
Afatinib	Gen 2	-8.66	-8.20	0.46	0.50	10.00	20.00	1.30
Dacomitinib	Gen 2	-8.46	-8.60	-0.14	6.00	60.00	10.00	1.00
Osimertinib	Gen 3	-8.15	-8.24	-0.08	493.80	11.40	0.02	-1.64

Evaluation of fold-changes. Erlotinib (Gen 1) experiences a 3.18 cell-line resistance ratio while Osimertinib (Gen 3) experiences a -1.64 cell-line ratio. Weak negative correlation confirms thermodynamic binding scores alone are not effective in proving inhibitor adaptation across generations.

Table 3: Hydrogen Bond Retention between Wild-type and Mutant Receptors

GEN	Inhibitor	Wildtype count	Mutant count	Wildtype H-Bonds (RES & DIST)	Lost H-Bonds (RES & DIST)	Gained H-Bonds (RES & DIST)
Gen 1	Erlotinib	1	0	THR854 (2.65Å)	THR854 (2.65Å)	None
Gen 1	Gefitinib	2	1	ARG841 (2.25Å), ASP855 (2.45Å)	ARG841 (2.25Å), ASP855 (2.45Å)	LYS745 (2.40Å)
Gen 2	Afatinib	1	0	MET793 (3.02Å)	MET793 (3.02Å)	None
Gen 2	Dacomitinib	1	0	CYS797 (2.39Å)	CYS797 (2.39Å)	None
Gen 3	Osimertinib	1	0	THR790 (2.31Å)	THR790 (2.31Å)	None

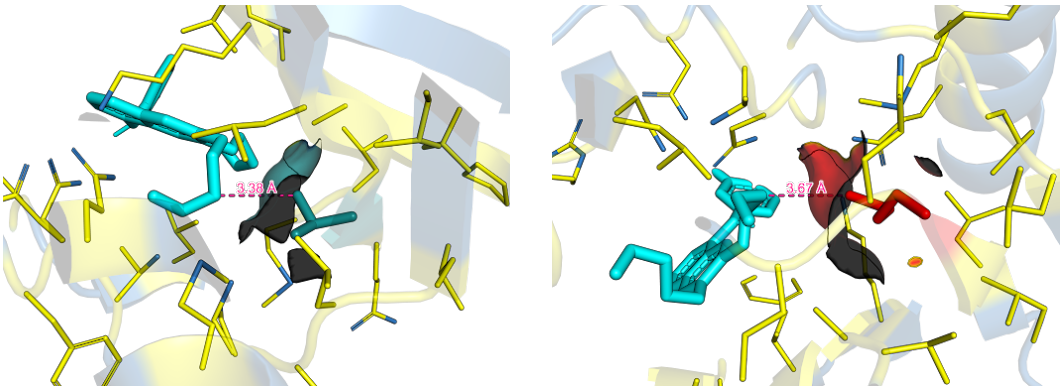
Threonine substituted with Methionine side chains result in significant van der Waals overlap. Nearest atomic clearance shrinks to 3.67 Å. This extremely tight boundary causes direct steric repulsion, physically pushing Erlotinib out of optimal alignment.

Unlike Erlotinib, Osimertinib's flexible core bypasses the gatekeeper barrier, resulting in an atomic clearance of 4.31 Å. Extended distance significantly mitigates van der Waals collisions, allowing Osimertinib to accommodate the Met790 side chain with minimal active-site distortion.

Table 4: Hydrophobic Contact Loss Summary

GEN	DRUG	Wildtype Hydrophobic contact count	Mutant Hydrophobic contact count	Wildtype Hydrophobic Residules	Lost hydrophobic contacts	Gained hydrophobic contacts
Gen 1	Erlotinib	4	3	ALA743, LEU718, LEU844, VAL726	ALA743, LEU718, LEU844	LEU858, PHE723
Gen 1	Gefitinib	1	5	LEU718	LEU718	ALA743, LEU844, LEU858, PHE723, VAL726
Gen 2	Afatinib	6	4	ALA743, LEU718, LEU844, LYS745, PHE723, VAL726	ALA743, LEU718, LYS745	None
Gen 2	Dacomitinib	5	2	ASP800, LEU844, PHE723, VAL726	ASP800, VAL726	None
Gen 3	Osimertinib	2	4	ASP800, PHE723	ASP800, PHE723	ALA743, LEU792, LEU844, PRO877

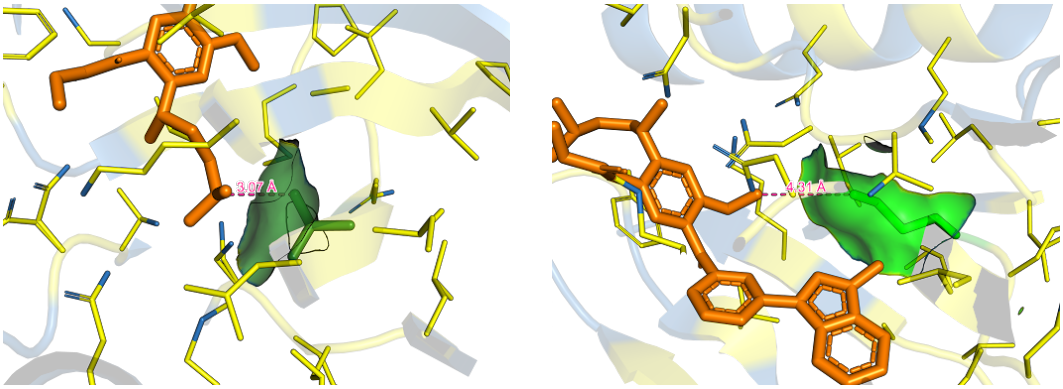
Figure 3: Erlotinib Active Site Clearance Comparisons



(a) Erlotinib Wild-type collision

(b) Erlotinib M790 collision

Figure 4: Osimertinib Active Site Clearance Comparisons



(a) Osimertinib Wild-type collision

(b) Osimertinib M790 collision

Table 5: Exhaust Convergence

Exhaustiveness	**Top free energy (ΔG) in kcal/mol**
2	-7.81
4	-8.175
8	-8.271
16	-8.271
32	-8.219

5 Discussions and Limitations

5.1 Docking $\Delta\Delta G$ scores

Standard molecular docking relies on binding free energy (ΔG) calculations to predict inhibitor efficacy, as ΔG represents thermodynamic favorability of inhibitor-receptor formation complexes. Consequently, it is reasonable to expect free energy scores to closely resemble an increase in inhibitor efficacy across generations. As shown in Table 1 and Figure 1, net thermodynamic shift upon mutated receptor ($\Delta\Delta G$) ranged from -0.30 to $+0.46$ kcal/mol, suggesting inhibitor generation exhibits minimal impact on binding potential across the mutant receptor. However, in Table 2 and Figure 2, cross-validating these results against experimental IC_{50} fold changes shows extremely weak correlations ($r = -0.12, p = 0.20$). This lack of convergence suggests that scalar binding energy analysis fails to account for inhibitor generation adaptations, highlighting the need for additional metrics to accurately validate the causes of generation adaptation.

5.2 PLIP analysis

PLIP analysis was conducted to detail the specific non-covalent interactions between each inhibitor and their EGFR receptor variants. Table 3 details the H-bond retention rates, showing that every inhibitor, regardless of generation, loses its wild-type H-bonds upon the mutated receptor, indicating H-bond retention rates do not prove inhibitor generation efficacy. However, Table 4 highlights key generational differences in inhibitor hydrophobic contacts. First-generation inhibitors undergo a reduction in their hydrophobic interactions (Erlotinib drops from 4 to 3, Gefitinib shifts to 5, though this reflects displacement rather than binding optimization) as well as Gen 2 inhibitors, though slightly less severe (Afatinib drops from 6 to 4, Dacomitinib drops from 5 to 2). In contrast, Third-generation inhibitor Osimertinib doubles its hydrophobic contact count (2 to 4), specifically establishing non-polar interactions across residuals Ala743, Leu792, Leu844, and Pro877. This increased hydrophobic packing in the binding cleft results in a phenomenon known as the hydrophobic effect, where the newly established non-polar contacts push polar water molecules out of the active site, creating a non-polar environment which locks the inhibitor in place to effectively block ATP access.

5.3 PyMOL analysis

PyMOL analysis utilizes 3D active site modeling to provide crucial insights in inhibitor-receptor complexes. Figure 3a details wild-type Erlotinib with a clearance distance of 3.38 Å between the T790 side chain and Erlotinib aniline ring while Figure 3b details mutant Erlotinib with a contact distance at 3.67 Å. While the mutant contact distance slightly increases, T790M's substitution of Methionine results in a bulkier side chain that extends into the binding cleft, resulting in optimal non-bonded van der Waals forces requiring $\sim$ 3.8–4.0 Å to prevent repulsion. Since the mutant Erlotinib contact distance is below the $\sim$ 3.8–4.0 Å threshold, van der Waals forces push Erlotinib out of its ideal binding position, leaving the active site open for ATP to enter and conduct unwanted cell signaling. Conversely, Figure 4a details wild-type Osimertinib clearance distance at 3.07 Å while Figure 4b details mutant Osimertinib contact distance at 4.31 Å. Since the mutant Osimertinib contact distance is above the $\sim$ 3.8–4.0 Å van der Waals threshold and still optimally within the active site (< 5.0 Å), Osimertinib successfully competes with ATP and blocks potential phosphorylation cascades, visually demonstrating the structural superiority third-generation inhibitors have over first-generation inhibitors.

5.4 Limitations

While this study effectively provides insight into inhibitor generation adaptation against mutated EGFR receptors, several limitations should be considered. AutoDock Vina was utilized for our docking script, which does not explicitly model covalent bond formation; interactions therefore reflect the pre-reaction non-covalent binding pose rather than the final complex, though this approach remains highly valid because correct non-covalent spatial positioning is a mandatory prerequisite for covalent bond formation. Additionally, our dataset was restricted to five TKIs evaluated against the wild-type and mutant EGFR receptor. Expanding this dataset to include additional TKIs and

receptors would provide broader insights, though these were not included due to computational costs and the current dataset providing a sufficient baseline for evaluating TKI evolution.

6 CONCLUSION

This study provided a computational evaluation of TKI generation adaptation against mutated EGFR receptors and the molecular mechanisms contributing to increased efficacy. Our study's findings showed that traditional docking energy calculations are ineffective for determining inhibitor adaptation, as scalar free-energy binding exhibited minimal variance ($\Delta\Delta G = -0.30$ to $+0.46$ kcal/mol) among inhibitor generations and failed to correlate with previously existing experimental IC_{50} data.

In contrast, PyMOL 3D active site analysis effectively modeled the structural basis of inhibitor generations across receptor states, providing a concrete visualization explaining inhibitor generation adaptation. Within the active site, first-generation inhibitors exhibit short contact distances from the mutant M790 side chain, resulting in van der Waals repulsion and steric hindrance that allow for unwanted ATP binding; conversely, third-generation inhibitors exhibit flexible contact distances, avoiding van der Waals repulsion while remaining in an optimal position in the active site to minimize ATP binding and subsequently decreasing unwanted ATP binding, whereas older generations decreased in hydrophobic contact and therefore failed to prevent potential ATP binding.

Further research should take into account an increase in the number of inhibitors utilized as well as multi-mutant EGFR receptor variants to expand the scope of this phenomenon as well as incorporating additional methods such as molecular dynamic simulations for additional analysis on the behavior of different generation inhibitors. Ultimately, this study's findings show the generational adaptation of inhibitors stems from spatial accommodation as well as an increase in hydrophobic contact.

REFERENCES

Anonymous Author(s). Inhibitor-mutation-research: Structural and thermodynamic evaluation of egfr t790m mutations. Anonymous Repository, 2026. URL https://anonymous.4open.science/r/Inhibitor-Mutation-Research-6304/.

D. A. Cross, S. E. Ashton, S. Ghiorghiu, C. Eberlein, C. A. Nebhan, P. J. Spitzler, and R. A. Ward. Azd9291, an irreversible egfr tki, overcomes t790m-mediated resistance to egfr inhibitors in lung cancer. *Cancer Discovery*, 4(9):1046–1061, 2014.

J. Eberhardt, D. Santos-Martins, A. F. Tillack, and S. Forli. Autodock vina 1.2.0: New docking methods, expanded force field, and python bindings. *Journal of Chemical Information and Modeling*, 61(8):3891–3898, 2021.

M. J. Eck and C. H. Yun. Structural and biochemical availability of mutant egfr in lung cancer. *Biochimica et Biophysica Acta (BBA)-Proteins and Proteomics*, 1804(3):559–566, 2010.

J. A. Engelman, K. Zejnullahu, C. M. Gale, E. Lifshits, A. J. Gonzales, T. Shimamura, and P. A. Jänne. Pf00299804, an irreversible pan-erbb inhibitor, is effective in models of egfr t790m-mediated resistance. *Cancer Research*, 67(24):11924–11932, 2007.

M. R. Finlay, M. J. Anderton, S. E. Ashton, P. A. Bethel, M. R. Box, R. H. Bradbury, and R. A. Ward. Discovery of 2-4-(1h-indol-3-yl)pyrimidin-2-ylamino-5-acetamidophenyl acrylamides as selective inhibitors of egfr t790m. *Journal of Medicinal Chemistry*, 57(20):8249–8267, 2014.

T. A. Halgren. Merck molecular force field. i. basis, form, scope, parameterization, and performance of mmff94. *Journal of Computational Chemistry*, 17(5-6):490–519, 1996.

S. Kobayashi, T. J. Boggon, T. Dayaram, P. A. Jänne, O. Kocher, M. Meyerson, and B. Halmos. Egfr mutation and resistance of non-small-cell lung cancer to gefitinib. *New England Journal of Medicine*, 352(8):786–792, 2005.

D. Li, L. Ambrogio, T. Shimamura, H. Ji, A. G. Sorensen, J. A. Engelman, and K. K. Wong. Bibw2992, an irreversible egfr/her2 inhibitor highly active in preclinical lung cancer models. *Oncogene*, 27(34):4702–4711, 2008.

T. J. Lynch, D. W. Bell, R. Sordella, S. Gurubhagavatula, R. A. Okimoto, B. W. Brannigan, and D. A. Haber. Activating mutations in the epidermal growth factor receptor underlying responsiveness of non-small-cell lung cancer to gefitinib. *New England Journal of Medicine*, 350(21):2129–2139, 2004.

T. S. Mok, Y. L. Wu, M. J. Ahn, M. C. Garassino, H. R. Kim, S. S. Ramalingam, and V. A. Papadimitrakopoulou. Osimertinib or platinum-pemetrexed in egfr t790m-positive lung cancer. *New England Journal of Medicine*, 376(7):629–640, 2017.

W. Pao, V. A. Miller, K. A. Politi, G. J. Riely, R. Somwar, M. F. Zakowski, and H. E. Varmus. Acquired resistance of lung adenocarcinomas to gefitinib or erlotinib is associated with a second mutation in the egfr kinase domain. *PLoS Medicine*, 2(3):e73, 2005.

F. Solca, G. Dahl, A. Zoephel, G. Bader, M. Sanderson, C. Klein, and F. Himmelsbach. Target binding properties of afatinib, an irreversible erbb family blocker. *Journal of Pharmacology and Experimental Therapeutics*, 343(2):342–350, 2012.

J. C. Soria, Y. Ohe, J. Vansteenkiste, T. Reungwetwattana, B. Chewaskulyong, K. H. Lee, and S. S. Ramalingam. Osimertinib in untreated egfr-mutated advanced non-small-cell lung cancer. *New England Journal of Medicine*, 378(2):113–125, 2018.

O. Trott and A. J. Olson. Autodock vina: Improving the speed and accuracy of docking with a new scoring function, efficient optimization, and multithreading. *Journal of Computational Chemistry*, 31(2):455–461, 2010.

R. A. Ward, M. J. Anderton, S. E. Ashton, P. A. Bethel, M. R. Box, S. Butterworth, and M. R. Finlay. Structure-guided design of a series of egfr tkis with high selectivity for the t790m mutation. *Journal of Medicinal Chemistry*, 56(17):7025–7048, 2013.

Y. Yarden and M. X. Sliwkowski. Untangling the erbb signalling network. *Nature Reviews Molecular Cell Biology*, 2(2):127–137, 2001.

C. H. Yun, T. J. Boggon, Y. Li, M. S. Woo, H. Greulich, M. Meyerson, and M. J. Eck. The t790m mutation in egfr kinase causes drug resistance by increasing atp affinity. *Proceedings of the National Academy of Sciences*, 105(6):2070–2075, 2008.

W. Zhou, D. Ercan, L. Chen, C. H. Yun, D. Li, M. Capelletti, and P. A. Jänne. Novel mutant-selective egfr kinase inhibitors against egfr t790m. *Nature*, 462(7276):1070–1074, 2009.